AIAA AVIATION Forum
August 2-6, 2021, VIRTUAL EVENT
AIAA AVIATION 2021 FORUM

10.2514/6.2021-3036

Adjoint-Based Uncertainty Quantification and Calibration of RANS-Based Transition Modeling

Reza Djeddi,* Coleman D. Floyd,† James G. Coder,‡ and Kivanc Ekici§
The University of Tennessee, Knoxville, Tennessee 37996

The main objective of the present study is to use a gradient-based optimization framework to perform uncertainty quantification and sensitivity analysis for the closure coefficients of the two-equation Amplification Factor Transport (AFT) model with the aim of improving its prediction capability. Additionally, the critical amplification factor, which directly controls the onset of the transition via the source term of the intermittency equation, is calibrated for a set of canonical flat plate test cases in both bypass and natural transitional regimes. It is shown that by utilizing a sigmoid fitting of the turbulence index profile, the transition onset location can be accurately predicted in a differentiable and smooth fashion that is essential to the adjoint-based sensitivity analysis of the RANS solver. Subsequently, the results of these calibration studies are used for obtaining a new relation via a high-order polynomial regression model that can define the critical amplification factor as a function of the free-stream turbulence intensity. Finally, the efficacy of the calibrated relation is tested for the natural laminar flow NLF(1)-0416 airfoil and the results show significant improvements in predicting the transition onset location as well as lift and drag predictions.

Nomenclature

C_f	skin friction coefficient
C_D	total drag coefficient
C_L	lift coefficient
c	chord length
d	distance to nearest wall point
E	total energy per unit mass
H_L	local boundary-layer shape factor
h	specific enthalpy
I	objective function
i_t	turbulence index (SA model)
L	reference length
M_∞	free-stream Mach number
$\vec{n}$	outward unit normal vector
$\tilde{n}$	modified amplification factor (AFT model)
p	pressure
Pr	Prandtl number
Re	Reynolds number
$\mathcal{R}$	residual of state variables
S	magnitude of strain rate tensor
$\tilde{S}$	limited or clipped magnitude of strain rate tensor

*Research Assistant Professor and Lecturer, Department of Mechanical, Aerospace and Biomedical Engineering, Professional Member AIAA.
†Graduate Student, Department of Mechanical, Aerospace, and Biomedical Engineering, Student Member AIAA.
‡Assistant Professor, Department of Mechanical, Aerospace, and Biomedical Engineering, Senior Member AIAA.
§Professor, Department of Mechanical, Aerospace and Biomedical Engineering, Senior Member AIAA.

t	time
u, v	Cartesian velocity components
x, y	Cartesian spacial components
$\mathbf{x}$	vector of design variables (closure coefficients)
y^+	non-dimensional distance from the first cell to the wall
α	angle of attack
γ , $\tilde{\gamma}$	original and modified intermittency
μ	dynamic viscosity
ν	kinematic viscosity (i.e. viscous diffusivity)
$\tilde{\nu}$	modified eddy viscosity (SA model)
ρ	density
τ	shear stress
σ , σ_n , σ_γ	turbulent Prandtl number (SA model) and its variants in the AFT model
χ	eddy viscosity ratio (SA model)
Ω	vorticity magnitude

I. Introduction

Today's computational limitations force most researchers and industry practitioners to take a statistical modeling approach to turbulent and transitional flows found in many engineering problems. Spatially averaging the sub-grid physics described by the Navier-Stokes equations remains the dominant strategy for complex flows and is likely to continue to be the case for decades to come. However, this computational affordability comes at a cost of uncertainty - due to neglecting the small scale turbulent fluctuations - and the issue of closure of the "Reynolds Stress" term. The most popular and pragmatic method for achieving closure employs the Boussinesq's assumption of linear dependence between the mean rate of strain and the Reynolds Stress. The variable used to define this linear relationship is the "eddy-viscosity", which is determined most commonly using single or multi-equation transport models (i.e. an eddy viscosity model), each having strengths and weaknesses due to their unique mathematical formulations of turbulent phenomena and consideration or omission of specific turbulent effects. These three aforementioned assumptions, i.e., Reynolds Averaging, the Boussinesq Conjecture, and the choice of the eddy viscosity model, all contribute to structural uncertainty and significantly stifle simulation accuracy and fidelity. This principle dilemma is a well-recognised challenge in the CFD community,[1] and its mitigation is the subject of ongoing research including but not limited to uncertainty quantification and reduction,[2] data-driven machine learning augmentation,[3,4] and model-form calibration through data-assimilation, to name a few.

Laminar-to-turbulent transition modeling is an effective strategy for improving the performance of well-established turbulence models which can be done via the coupling of additional governing equations to the eddy viscosity model in order to predict the transition onset location, the extent of the transitional region, as well as downstream re-laminarization (if present). Obviously, the improved accuracy and prediction capability comes at the price of increased computational cost due to the inclusion of the additional transition model equations. For example, the widely-used one-equation linear eddy viscosity (LEV) model due to Spalart and Allmaras[5,6] has been coupled with a multitude of different transition models that have proven to greatly enhance the boundary layer prediction capabilities. In general, the inclusion of a transition model alleviates a component of the aforementioned structural uncertainty that originates from the assumption of a fully turbulent boundary-layer which is a known falsehood for large regions of external flows past aerodynamic and hydrodynamic bodies. Therefore, transition models show the potential to recover prediction accuracy of important flow characteristics, namely skin friction, heat transfer, and boundary layer separation. Despite these benefits and a considerable amount of well-established theoretical and empirical knowledge of the laminar-to-turbulent transition process, development and inclusion of compatible transition models in CFD simulations has mostly taken place within the last decade. This is attributed to CFD codes preventing the use of non-local operations in addition to the physical complexity of the subject which is mostly associated with the fact that the boundary layer transition is a multi-stage process with multiple potential mechanisms/paths to turbulence and thus, can be triggered by one or a combination of factors (e.g. high free-stream turbulence, adverse pressure gradients, crossflow, compressibility, or even surface vibration, roughness, and curvature).[7]

A few different approaches have been developed in the recent years that incorporate the prediction of

laminar-to-turbulent transition phenomenon into existing RANS solvers.[8–18] Arnal et al.[19] and Medida[20] provide good reviews of different transition modeling techniques as well as the advantages and disadvantages of each method in detail. In general, there are two main classes of transition modeling techniques: (1) those based on a stability analysis and a critical amplification criterion (i.e. the e^N method), and (2) those based on empirical correlations of transition onset. In the former approach, linear stability theory is used to approximate the growth of disturbances in the boundary layer and based on a critical value of amplification ratio, transition onset can be determined (see Refs.[21,22]). Transition onset functions, on the other hand, are based on correlations determined from experimental data and offer relatively accurate predictions within their calibration database.[23–25] While most of these empirically-based transition models use integral boundary layer properties to define transition onset, Langtry and Menter[10] have introduced the $\gamma - \overline{\mathrm{Re}_{\theta t}}$ model that uses correlations based on local flow properties. While this model was originally introduced for the k-ω SST turbulence model,[26] it has since been tailored[27] to work with the Spalart-Allmaras[5] turbulence model. More recently, a zero-equation transition model has been proposed by Bas and Cakmakcioglu[28] that offers relatively accurate predictions of transition onset, separation and reattachement zones without the need to solve an additional transport equation. This correlation-based algebraic transition model uses an intermittency distribution function based on the local information and can handle high freestream turbulence intensities. Another important and interesting feature of this transition model is that there are only two calibration parameters involved in the transition onset function which can be optimized for different applications.

From wind turbines to helicopter rotors to transport aircraft, most aerodynamic bodies within the subsonic and transonic regimes experience *natural transition*. Conveniently, stability theory adequately captures this process of primary to secondary instabilities (e.g. Tollmien-Schlichting waves progressing to three-dimensional waves and vortices) followed by breakdown then turbulent formations stemming from surface tripping points.[29] Using the e^N empirically-based correlation method[30,31] of linear stability analysis, Coder and Maughmer[32] formulated the Amplification Factor Transport transition model (AFT2014), which is coupled to the Spalart-Allmaras LEV model by the transported envelope amplification factor, $\tilde{n}$. Studied herein, is the more robust version of the AFT transition model (AFT2019)[33] which solves a second transport equation for the modified intermittency, $\tilde{\gamma}$, describing the switch from the laminar regime to the turbulent regime. Compared to the popular four-equation k-ω-γ-$\mathrm{Re}_{\theta t}$ SST turbulent transition model developed by Langtry and Menter[34] (which favors high freestream turbulent intensity; applicable to internal turbine cascades), the less expensive three-equation AFT2019 and Spalart-Allmaras model is capable of modeling a broad class of external flows subject to natural transition.

Looking deeper into the formulation of a joint turbulent-transition model, beyond the *structural uncertainty*, there is *parametric uncertainty*, considered the "fourth level" of uncertainty by Duraisamy et al.[3] Being the focus of this paper, parameter uncertainty originates from the closure coefficients embedded in the equations of both the turbulence and transition models, which are responsible for scaling functions and terms. Values of these coefficients require *a priori* specification and are commonly adopted as the "standard values" recommended by the model creators. The relevant literature is in clear agreement that there is no universal set of optimal closure coefficient values for turbulence modeling, nor are optimal values necessarily constant across domains of space and time.[35] This limitation may be assumed applicable for transition models as well since the transition process is less universal than commonly accepted for turbulence. Standard values are calibrated during model formulation to produce acceptable but compromised agreement for a range of simplistic canonical flow cases with respect to experimental results and/or high fidelity numerical data. Despite structural uncertainties being the roots for under performing LEV models and their transition extensions, case-specific parameter calibration of the closure coefficients is known and shown herein to counterbalance portions of the structural/model-form deficiencies. Moreover, addressing uncertainties through model parameters allow for efficient non-intrusive methods, as opposed to the more complex strategies for performing structural uncertainty quantification and mitigation.

Since the start of the century, the literature shows growing attention to sensitivity and uncertainty of the epistemic coefficients of LEV turbulence models and more recently to their transition extensions. Both deterministic and statistical approaches have been developed, each with strengths and disadvantages. However, works involving the deterministic approach of specifically using automatic differentiation algorithms to compute the sensitivities of the closure coefficients has been absent from the literature for more than a decade despite their efficiency. On the other hand, studies employing probabilistic approaches (e.g., Bayesian maximum a posteriori estimates[36,37]) and stochastic approaches (e.g., surrogate-based spectral

methods[38–41]), have been multiplying as of recent.

The objective of the present study is to perform uncertainty quantification and sensitivity analysis for the closure coefficients of the two-equation Amplification Factor Transport (AFT) model using a gradient-based optimization framework with the goal of improving the transition prediction capabilities. In addition to this, the value of the critical amplification factor is calibrated for a set of canonical flat plate test cases in both bypass and natural transitional regimes. It must be noted that this parameter controls the onset of the transition via the source term of the intermittency equation and our numerical results have shown a significant improvement in the transition prediction accuracy when this critical factor is calibrated. In order to accurately predict the onset location, a sigmoid function is fitted to the turbulence index profile. It is important to note that this approach is crucial in obtaining a differentiable and smooth objective function for the calibration problem. Ultimately, the results of the calibration studies for the critical amplification factor are used in determining a new relation, similar to that of Mack[42] and Drela[43] that can give the critical factor as a function of the free-stream turbulence intensity. The efficacy of the calibrated relation is tested for the natural laminar flow NLF(1)-0416 airfoil. Our numerical results have shown a significant improvement in the transition onset location as well as lift and drag predictions by utilizing the calibrated critical amplification factor for this natural transitional case. To the best of authors' knowledge, this is the first work reported in the literature to: 1) perform sensitivity/uncertainty analysis of the closure coefficients in a transition model using a non-statistical approach, and 2) conduct calibration of the critical amplification factor using a gradient-based optimization based on the discrete adjoint form of the RANS equations.

II. Mathematical Formulation

In this section, details of the Amplification Factor Transport (AFT) transition model as well as the Spalart-Allmaras turbulence model are presented. Moreover, numerical considerations for "smoothing" the transition model are presented to enable the gradient-based inverse design optimization aimed at calibrating the closure coefficients of the AFT model as well as the critical amplification factor. Additionally, the coupling of the transition and turbulence models is described and numerical details of the inverse design problem are presented.

A. Transition Modeling Equations

The basis for the AFT transition model is the solution of a surrogate variable, $\tilde{n}$, called the modified amplification factor, which characterizes the envelope of linearly amplified instabilities throughout the boundary layer. The main advantage of the AFT model that sets it apart from other widely used transition models is that it is built on the premise that integral boundary layer (IBL) quantities, such as shape factor, are estimated using local surrogates. This estimation process relies on the carefully guided calibration of the AFT model closure coefficients based on the fundamental boundary-layer theory. In this work, however, we first focus on calibrating these closure coefficients based on experimental data with the goal of improving transition prediction capabilities of the AFT model. Details of the additional transport equations solved for the AFT model are presented in the following sections.

1. *Amplification Factor Transport*

Originally developed by Coder and Maughmer,[44] the AFT model focuses on solving a transport equation for the approximate envelope amplification factor such that

$$\frac{\partial \rho \tilde{n}}{\partial t} + \underbrace{\frac{\partial \rho u_j \tilde{n}}{\partial x_j}}_{\text{convective flux}} - \underbrace{\frac{\partial}{\partial x_j}\left[\sigma_n \left(\mu + \mu_t\right) \frac{\partial \tilde{n}}{\partial x_j}\right]}_{\text{diffusive flux}} = \underbrace{\rho \Omega F_{\text{crit}} F_{\text{growth}} \frac{d\tilde{n}}{d\text{Re}_\theta}}_{\text{source term}} \tag{1}$$

While details of the AFT transition model are presented in Ref.,[33] for completeness, the definitions of each individual term in the governing equations of the AFT model will be presented in this work. As discussed earlier, the boundary-layer methods rely on the availability of the integral momentum thickness as well as the integral shape factor to determine the boundary-layer profile. However, the AFT model focuses on "estimating" the integral properties using a *local shape factor*. This local shape factor that was originally proposed in the AFT2017a model[45] is defined as

$$H_L = \frac{d^2}{\mu}\left[\nabla\left(\rho\vec{u}\cdot\nabla d\right)\cdot\nabla d\right] \tag{2}$$

where d is the shortest distance from wall and the gradient of the wall distance in Eq. (2) is a reflection of the wall-normal derivative of the wall-normal momentum as a Galilean-invariant indicator of streamwise velocity gradient. Additionally, the gradient factor described in the definition of the H_L is an indicator of the free-stream pressure gradient. It is important to note that H_L must be limited within $[-0.25, 200]$ for numerical stability. Finally, the integral shape factor, H_{12}, can be estimated by

$$H_{12} = \min\left[\max\left(0.26H_L + 2.4, 2.2\right), 20.0\right] \tag{3}$$

where the lower bound of 2.2 tries to keep the estimated shape factor in a physically reasonable range while preventing any unintentional destruction of the approximate envelope (or the amplification factor) that is being transported by the model. On the other hand, the estimated integral shape factor, H_{12}, is also bounded by an upper limit of 20.0 that is used to avoid any non-physical production through shock waves, discontinuities, and in the vicinity of stagnation points.

Having the local shape factor, the growth of the amplification factor can be defined according to the AFT2017a and AFT2019 models based on the assumption of a fixed H_{12} value, i.e., local self-similarity. This growth term is defined as the variations of the amplification factor with respect to the momentum-thickness Reynolds number[44] such that

$$\frac{d\tilde{n}}{d\mathrm{Re}_\theta} = 0.028\left(H_{12}-1\right) - 0.0345\exp\left[-\left(\frac{3.87}{H_{12}-1} - 2.52\right)^2\right] \tag{4}$$

As can be seen, it is not necessary to explicitly evaluate the momentum-thickness Reynolds number, Re_θ, as it is done in the Langtry and Menter[34] two-equation transition model. Additionally, the AFT model focuses on estimating the growth of the boundary layer through a F_{growth} function in the source term of the $\tilde{n}$-transport equation which is described as a function of the local shape factor via

$$F_{\mathrm{growth}} = \left[\frac{2.4H_{12}}{H_{12}-1}\right]\frac{1+m(H_{12})}{2}\,l(H_{12}) \tag{5}$$

where $m(H_{12})$ and $l(H_{12})$ are defined according to Drela and Giles[46] as

$$l(H_{12}) = \frac{6.54H_{12} - 14.07}{H_{12}^2} \tag{6}$$

$$m(H_{12}) = \frac{1}{l(H_{12})}\left[0.058\frac{(H_{12}-4)^2}{H_{12}-1} - 0.068\right] \tag{7}$$

Probably one of the most important terms in the amplification factor transport equation is a step function called, F_{crit}, which toggles from 0 to 1 as a function of the local vorticity Reynolds number defined as

$$\mathrm{Re}_\nu = \frac{\rho S d^2}{\mu + \mu_t} \tag{8}$$

where S is the magnitude of the strain rate tensor and μ_t is the turbulent eddy viscosity. The value of the critical function becomes 1 when the local vorticity Reynolds number reaches a critical threshold, $\mathrm{Re}_{\nu,0}$, which is correlated to the transition momentum-thickness Reynolds number by a function of the integral shape factor H_{12},[33,47] such that

$$F_{\mathrm{crit}} = \begin{cases} 0, & \mathrm{Re}_\nu < \mathrm{Re}_{\nu,0} \\ 1, & \mathrm{Re}_\nu \geq \mathrm{Re}_{\nu,0} \end{cases} \tag{9}$$

Note that the step function described above is non-smooth and non-differentiable at $\mathrm{Re}_\nu = \mathrm{Re}_{\nu,0}$ which will be the focus of the "smoothing" procedure that will be described later in this work. This smoothing process would be essentially important in order to enable gradient-based design problems involving the AFT transition model. It is also important to note that there are no *tunable* closure coefficients in the amplification factor transport equation source term.

2. Intermittency Transport

Unlike the earlier versions of the AFT model, i.e., AFT2014[44] and AFT2017a,[45] where an algebraic intermittency was being used for suppressing turbulence production in the laminar boundary layers, the AFT2017b[48] and later, the AFT2019[33] versions, utilized a transport equation for the modified intermittency, $\tilde{\gamma}$, which is a mapping of the actual intermittency via

$$\tilde{\gamma} = \ln(\gamma) \tag{10}$$

where γ is 0 in laminar regions but 1 in turbulent regimes.[34] In this work, however, we focus on solving a slightly modified version of the AFT2019 transition model where we solve the transport equation (second governing equation of the AFT model) for the actual intermittency instead. This transport equation is described below

$$\frac{\partial \rho\gamma}{\partial t} + \underbrace{\frac{\partial \rho u_j \gamma}{\partial x_j}}_{\text{convective flux}} - \underbrace{\frac{\partial}{\partial x_j}\left[\left(\mu + \frac{\mu_t}{\sigma_\gamma}\right)\frac{\partial \gamma}{\partial x_j}\right]}_{\text{diffusive flux}} = \underbrace{c_1 \rho S F_{\text{onset}}\left(1-\gamma\right)}_{\text{production source term}} - \underbrace{c_2 \rho \Omega F_{\text{turb}}\left(c_3\gamma - 1\right)}_{\text{destruction source term}} \tag{11}$$

As can be seen in Eq. (11), there are two main functions that are described in the production and destruction source terms of the intermittency transport equation. The first function, which determines the onset of the transition, is described as balance between two different behaviors that are used to control the intermittency. The first measure, focuses on transition criterion and whether or not it has been satisfied such that

$$F_{\text{onset},1} = \frac{\tilde{n}}{N_{\text{crit}}} \tag{12}$$

where $\tilde{n}$ is obviously the modified amplification or envelope factor determine via the first governing equation of the AFT model and N_{crit} is the critical amplification factor based on the linear stability theory[33] which will be described later. Ultimately, the $F_{\text{onset},1}$ function is limited with an upper bound of 2.0 as originally proposed in the one-equation Menter model[49] to prevent excessive amount of production in the intermittency equation, i.e.,

$$F_{\text{onset},2} = \min\left(F_{\text{onset},1}, 2.0\right) \tag{13}$$

On the other hand, the second mechanism involved in the onset function focuses on the presence of turbulence in the boundary layer which should theoretically affect the production of the intermittency. Therefore, we have

$$F_{\text{onset},3} = \max\left[1 - \left(\frac{R_T}{3.5}\right)^3, 0\right] \tag{14}$$

where R_T is the ratio of the eddy viscosity to the laminar viscosity, i.e., $R_T = \mu_t/\mu$, which is also known as the characteristic turbulence Reynolds number. Finally, the onset function in the production source term of the intermittency equation is defined as

$$F_{\text{onset}} = \max\left[F_{\text{onset},2} - F_{\text{onset},3}, 0\right] \tag{15}$$

Ultimately, the destruction source term of the intermittency equation is controlled by a F_{turb} function which tries to prevent destruction of intermittency within an already turbulent boundary layer based on the value of R_T. As a matter of fact, the F_{turb} promotes laminarization in boundary layers with small turbulence Reynolds number while maintaining intermittency in turbulent boundary layers with large values of R_T. As a result, the F_{turb} is defined as[33]

$$F_{\text{turb}} = \exp\left[-\left(\frac{R_T}{2}\right)^4\right] \tag{16}$$

It is very important to note that the F_{turb} can in some cases inadvertently suppress the turbulence in the viscous sublayer due to the local nature of the turbulent Reynolds number. However, this issue will be handled primarily by the turbulence model and the details of this will be described later in this work

when the turbulence and transition models are coupled together. Another important issue to address is the number of minimum and maximum functions in the definition of the intermittency source term. These functions are also non-smooth and non-differentiable at their inflection point which will be addressed in the following section.

3. Smooth Version of the AFT Model

As discussed earlier in the definition of the original AFT model, the switching step function as well as the minimum and maximum functions are non-smooth and discontinuous. This means that these functions must be modified in order to smooth the AFT model and make it compatible with the gradient-based design optimization. This smoothing process is described in this section. The first function that will be addressed is the F_{crit} step function that, as shown earlier, simply enable or disable the entire source term for the amplification factor transport equation. For this reason, a modified hyperbolic tangent function, slightly similar to what proposed by Halila et al.,[50] is used in this work such that

$$F_{\text{crit}}^{\text{smooth}} = \frac{1}{2}\left[1 + \tanh\left(f_{\text{step}}\left(\text{Re}_{\nu} - \text{Re}_{\nu,0}\right)\right)\right] \tag{17}$$

where f_{step} is set to 500.[50]

Additionally, the minimum and maximum functions must be made smooth as these functions are used substantially in the calculation of the source terms for both of the AFT model equations. Moreover, the minimum and maximum functions are also used in the turbulence model and "smoothing" them would be essentially important for the compatibility of these models with gradient-based design optimization. In this work, the Kreisselmeier-Steinhauser (KS) function[51,52] is used to smooth the minimum and maximum functions. It must be noted that the KS functions are used to smooth min and max functions that arise in various mathematical applications involving a series of *measure* functions. Without getting into details, the final form of the "smooth" minimum and maximum functions are presented herein:

$$\min\left(\lambda_1, \lambda_2\right) = \frac{\ln\left[\exp(f_{\min}\lambda_1) + \exp(f_{\min}\lambda_2)\right]}{f_{\min}} \tag{18}$$

$$\max\left(\lambda_1, \lambda_2\right) = \frac{\ln\left[\exp(f_{\max}\lambda_1) + \exp(f_{\max}\lambda_2)\right]}{f_{\max}} \tag{19}$$

where $f_{\min}$ and $f_{\max}$ are normally in a range of $\pm[5, 200]$. This means that normally we have $f_{\min} = -100$ and $f_{\max} = +100$ to enable a smooth transition at the inflection point of the minimum and maximum functions.[50] It is important to note that the KS functions used here for smoothing the minimum and maximum functions rely on "normalized" arguments, i.e., $\lambda \approx \mathcal{O}(1)$. Therefore, to generalize the smooth form of the min and max functions described in Eqs. (18) and (19), the $f_{\min}$ and $f_{\max}$ parameters are set in a dynamic fashion depending on the order of magnitude of the two arguments, λ_1 and λ_2, involved in the minimum or maximum function.

4. Critical Amplification Factor

In the Langtry-Menter transition model,[34] the value of the free-stream turbulence intensity is used to determine the critical momentum-thickness Reynolds number, $\text{Re}_{\theta,c}$, through special correlations, such as Abu-Ghannam/Shaw criterion,[25] to determine the onset of transition. It must be noted that these correlations have been carefully calibrated for various test cases based on the experimental results and there is ongoing research in this area to improve such correlations.[53–55] In the AFT transition model, however, the free-stream turbulence intensity (FSTI) is used for determining the critical amplification factor, N_{crit}, that directly controls the onset function in the source term of the intermittency equation (see Eq. [12]). This critical factor is directly related to the free-stream turbulence intensity according to the modified[43] Mack's relationship[42]

$$\begin{aligned} N_{\text{crit}} &= -8.43 - 2.4\ln\left(\frac{\tau}{100}\right) \\ \tau &= 2.5\tanh\left(\frac{\text{Tu}\%}{2.5}\right) \end{aligned} \tag{20}$$

where τ is a smooth maximum function designed for preserving the positive values of the critical amplification factor and Tu% is the free-stream turbulence intensity described in "percent" value.

It is important to note that the free-stream turbulence intensity is defined as the ratio of the standard deviation of the mean velocity to the mean velocity (commonly reported in percent value). Therefore, in many experimental studies and wind tunnel data, the value of the FSTI is calculated very accurately by relying on free-stream velocity data typically measured using a constant temperature anemometer (CTA)[56] or laser velocimeters.[57] On the other hand, in many RANS-based transition prediction studies, the discrepencies between the CFD solutions and the experimental data are normally alleviated by manually "tuning" the turbulence intensity (FSTI).[28,32,50,58–60] In the case of the transition models based on the linear stability theorem, e.g., the e^N[30] or the AFT models,[32,33] this variation of the FSTI value is analogous to the variations of the critical amplification factor, N_{crit}. Therefore, in this work, the goal is to focus on calibrating the critical amplification using a gradient-based optimization of the transition onset location in order to resolve the discrepancies between CFD predictions and the experimental data. Ultimately, the calibrated amplification factors for a set of canonical test cases can be used for determining a "new" relation, similar to Eq. (20). This new relation can be obtained using a polynomial-based regression model and can be tuned for a wide range of transitional boundary layers including both bypass and natural transition processes.

B. Turbulence Model

The AFT model described in this work, is developed with the main intention of being used in conjunction with the one-equation turbulence model of Spalart and Allmaras (SA).[5] Therefore, details of the SA turbulence model and its coupling with the AFT transition model are presented in this section.

1. Spalart-Allmaras Model

The Spalart-Allmaras turbulence model used in this work is defined in its conservative form[6] as

$$\begin{aligned}\frac{\partial \rho\tilde{\nu}}{\partial t} + \underbrace{\frac{\partial \rho u_j \tilde{\nu}}{\partial x_j}}_{\text{convective flux}} - \underbrace{\frac{1}{\sigma}\left[\frac{\partial}{\partial x_j}\left(\rho(\nu+\tilde{\nu})\right)\frac{\partial \tilde{\nu}}{\partial x_j}\right]}_{\text{diffusive flux}} &= \underbrace{\rho c_{b1}\left(1-f_{t2}\right)\tilde{S}\tilde{\nu}}_{\text{production source term}} \\ \underbrace{-\rho\left[c_{w1}f_w - \frac{c_{b1}}{\kappa^2}f_{t2}\right]\left(\frac{\tilde{\nu}}{d}\right)^2}_{\text{destruction source term}} &+ \underbrace{\frac{1}{\sigma}\left[\rho c_{b2}\frac{\partial \tilde{\nu}}{\partial x_i}\frac{\partial \tilde{\nu}}{\partial x_i} - (\nu+\tilde{\nu})\frac{\partial \rho}{\partial x_i}\frac{\partial \tilde{\nu}}{\partial x_i}\right]}_{\text{diffusion source term}}\end{aligned} \tag{21}$$

where $\tilde{S}$ is the "limited" magnitude of the strain rate tensor to avoid having it reach zero or to become negative.[6] In the present work and as recommended by Coder,[33] the *negative* version of the Spalart-Allmaras, i.e., SA-neg, is being used. The SA-neg model is identical to the "standard" model whenever the modified eddy viscosity, $\tilde{\nu}$ is greater than or equal to zero. However, for cases where $\tilde{\nu}$ becomes negative, instead of clipping the turbulence model solution, the source terms are slightly varied and the following equation is solved instead:

$$\begin{aligned}\frac{\partial \rho\tilde{\nu}}{\partial t} + \underbrace{\frac{\partial \rho u_j \tilde{\nu}}{\partial x_j}}_{\text{convective flux}} - \underbrace{\frac{1}{\sigma}\left[\frac{\partial}{\partial x_j}\left(\rho(\nu+\tilde{\nu}f_n)\right)\frac{\partial \tilde{\nu}}{\partial x_j}\right]}_{\text{diffusive flux}} &= \underbrace{\rho c_{b1}\left(1-c_{t3}\right)\Omega\tilde{\nu}}_{\text{production source term}} \\ + \underbrace{\rho c_{w1}\left(\frac{\tilde{\nu}}{d}\right)^2}_{\text{destruction source term}} &+ \underbrace{\frac{1}{\sigma}\left[\rho c_{b2}\frac{\partial \tilde{\nu}}{\partial x_i}\frac{\partial \tilde{\nu}}{\partial x_i} - (\nu+\tilde{\nu})\frac{\partial \rho}{\partial x_i}\frac{\partial \tilde{\nu}}{\partial x_i}\right]}_{\text{diffusion source term}}\end{aligned} \tag{22}$$

It is important to notice that the sign of the destruction term is "positive" for the modified equation being solved in the SA-neg model for $\tilde{\nu} < 0$ cases (Eq. [22]), as opposed to the standard model. Moreover, the "limited" magnitude of the strain rate tensor, $\tilde{S}$, is replaced with the vorticity magnitude, Ω, in the production term of Eq. (22). Additionally, the f_n function used in the diffusive flux is described as

$$f_n = \frac{c_{n1} + \chi^3}{c_{n1} - \chi^3} \tag{23}$$

where $\chi = \tilde{\nu}/\nu$ and $c_{n1} = 16$.[6] Note that the rest of the closure coefficients and settings are identical to those from the standard model, details of which are provided in Ref.[5]

2. Coupling of Turbulence and Transition Models

As can be seen, the SA-Standard or the SA-neg models described in the previous section, utilize a "tripping" function, f_{t2}, in the definition of their production and destruction source terms. The goal of the f_{t2} function in the SA model, by design, has been to provide a tripping effect at the transition onset as well as a laminarization effect for small $\tilde{\nu}$ solutions. Therefore, the AFT2019 model tries to exploit this built-in functionality by modifying the f_{t2} term to include the solution of the AFT model intermittency equation such that

$$f_{t2} = c_{t3}\,(1 - \gamma) \tag{24}$$

where $c_{t3} = 1.2$ according to the SA model.[5,33] Additionally, the baseline values for the closure coefficients of the standard AFT model are described and presented in Table 1. These values will be used as the starting point to initiate the calibration process followed in this work based on the experimental data and an inverse design approach.

Table 1. Baseline closure coefficients used in the AFT transition model[33]

Coefficient	c_1	c_2	c_3	σ_n	σ_γ
Value	100.0	0.06	50.0	1.0	1.0

Another important aspect in the implementation of the AFT model and its coupling with the underlying SA turbulence model is to address numerical and stability considerations. Solutions to the amplification factor as well as the intermittency equations must be bounded to avoid spurious or non-physical solutions appearing in the flow field. In this work, the value of $\tilde{n}$ is bound within $[-1, 20]$ at the end of each time-step. Similarly, the value of the intermittency, γ, is bound within $[0, 1]$. In addition to these lower and upper bounds for the AFT model solutions, the maximum change for both $\tilde{n}$ and γ is also limited to 50% relative to their values at the previous step.[47] This residual limiting is found to be essential for promoting a good convergence behavior for the AFT model.

Finally, the transport equations solved for the SA turbulence model as well as the AFT transition model also require a proper boundary condition treatments. In general, the SA model uses a Dirichlet boundary condition at both far-field and wall boundaries where $\tilde{\nu}$ is set to zero at viscous walls while being set according to a user-specified eddy viscosity ratio, χ_∞, at inflow and far-field boundaries. For the standard SA model used for "fully-turbulent" test cases, the recommended value of χ_∞ is between 3.0 to 5.0.[5,6] However, in order to avoid saturating the incoming flow in the transitional cases, a smaller value of 0.1 is recommended for χ_∞ when AFT transition model is being utilized. Moreover, the AFT transition model uses a Dirichlet boundary condition for both $\tilde{n}$ and γ at the inflow and far-field with $\tilde{n} = 0.0$ and $\gamma = 1.0$ while using a Neumann condition at outflow and viscous wall boundaries.

C. Calibration Based on an Inverse Design Problem

The main goal of the present work is to re-calibrate the AFT transition model in order to improve the accuracy of its prediction for the transitional boundary layer. To achieve this goal, experimental data available for various benchmark test cases will be used in a gradient-based inverse design problem. The inverse design optimization uses the closure coefficients of the AFT model as the design variables and tries to minimize the prediction errors defined as the difference between numerical and experimental results. Therefore, the choice of the objective function or the quantity of interest in such an inverse design problem would be crucial. To motivate the minimization problem used in this work, let us assume the goal is to match the target transition onset location from the experimental study, such that

$$\min_{\mathbf{x}} \quad I = \frac{1}{2}\left(x_{\text{cr}} - x_{\text{cr}}^{\text{target}}\right)^2 \tag{25}$$

where $\mathbf{x}$ is the vector of design variables that includes all the closure coefficients described earlier for the AFT transition model. Additionally, x_{cr} and $x_{\text{cr}}^{\text{target}}$ are the critical or the transition onset locations from the

numerical and experimental studies, respectively. The remaining task would be to define a robust approach for determining the exact location of the transition onset. One choice which will be studied in this work is to rely on the "turbulence index" proposed by Spalart and Allmaras in their seminal work.[5] This index is defined as

$$i_t = \frac{1}{\kappa u_\tau} \frac{\partial \tilde{\nu}}{\partial n} \tag{26}$$

where wall shear velocity, u_τ, is approximated as $u_\tau \approx \sqrt{\nu \Omega}$, and n is the wall-normal direction. The turbulence index described in Eq. (26) will have a value close to zero in laminar regions while switching rapidly to a value close to one in turbulent regions. According to Spalart and Allmaras,[5] the value of i_t can rise slightly above one in the turbulent boundary layer as it approaches separation. The goal here is to utilize this turbulence index as a measure to determine the onset or critical location, x_{cr}, that can be used in the definition of the quantity of interest described in Eq. (25). For the purpose of the gradient-based design optimization, it is essential to have a differentiable path between the objective function and the set of design variables as well as flow solution. Therefore, in this work, a non-linear least-squares minimization problem is utilized to fit a sigmoid function to the turbulence index profile. The process is shown in Fig. (1) for a typical turbulence index profile where the transition onset location is determined based on the location at which the turbulence index reaches a value of $i_t = 0.5$.

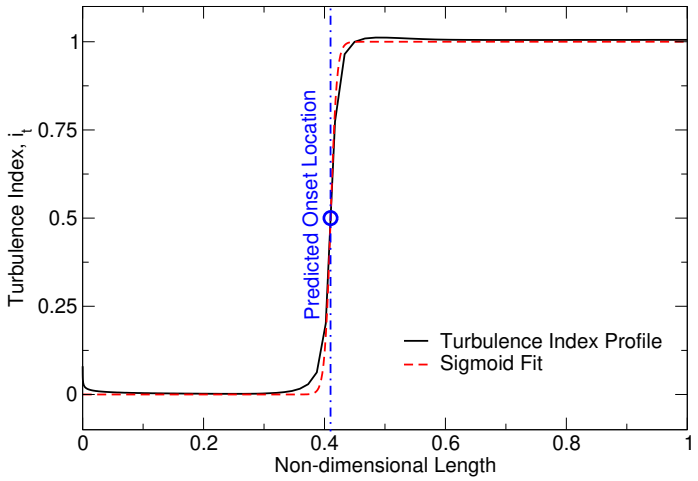

Figure 1. Turbulence index profile and the fitted sigmoid function based on a non-linear least-squares minimization. Notice the transition onset location predicted at $i_t = 0.5$ which also happens to be where the value of the sigmoid function reaches 0.5.

It must be noted that another choice for the objective function in these types of calibration problems would be the L2-error of the skin friction profiles between the CFD solver and the experimental measurements. However, the skin friction data for most experimental studies do not cover the entire span of the viscous wall which can create discontinuities in the objective function. Therefore, as will be shown later in this work, the choice of the turbulence index profile with the sigmoid fit used for determining the onset location is a very viable and accurate option that also leads to a smooth and continuous design space. Finally, the inverse design problem is solved using discrete adjoint-based optimization within our in-house UNstructured PArallel Compressible Design Optimization Framework (UNPAC-DOF).[61,62]

III. Uncertainty Quantification and Calibration of the AFT Transition Model

As the first step in calibrating the AFT transition model, an uncertainty quantification and sensitivity analysis is performed to identify the most sensitive closure coefficients of the model that directly affect the transition behavior. Results obtained in this section will guide us for calibrating the AFT model which will be discussed next.

A. Uncertainty Quantification and Sensitivity Analysis

For the purpose of uncertainty quantification (UQ), the modified T3A zero pressure gradient flat plate test case is considered. The flow settings for this case are according to the guidelines for "Case 1" from the AIAA Transition Modeling and Prediction Workshop (TMW) with a free-stream Mach number of 0.2 and a zero degree angle of attack. The Reynolds number per grid unit is 200,000 and the free-stream turbulence intensity is 5.855% which corresponds to a critical amplification factor of $N_{\text{crit}} = 0.467$ according to Eq. (20). Moreover, the eddy viscosity ratio is set to $\chi_\infty = 0.1$ in the free-stream.

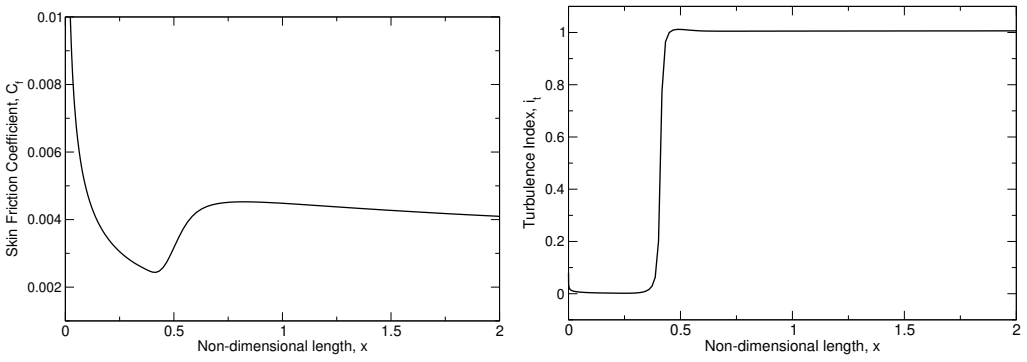

(a) Skin Friction Coefficient

(b) Turbulence Index

Figure 2. Skin friction coefficient and turbulence index distributions on the surface of the flat plate wall for the modified T3A case with zero pressure gradient (Tu = 5.855%).

The computational domain for this case extends for 0.25 units upstream of the leading edge of the flat plate and 5.0 units in the wall-normal direction. Additionally, the flat plate is extended for 20 units due to the low Reynolds number condition of the T3A test case. The computational grid has a total of 353×193 nodes with 256 nodes along the length of the flat plate. An inlet boundary condition is prescribed with $M_\infty = 0.2$ which corresponds to total pressure and total temperature ratios of $p_t/p_{\text{ref}} = 1.02828$ and $T_t/T_{\text{ref}} = 1.008$ while an outlet condition with $p/p_{\text{ref}} = 1.0$ is imposed at the exit of the computational domain. A Riemann-based far-field boundary condition is also imposed on the top boundary. Finally, a symmetry condition is applied upstream of the flat plate and the adiabatic solid wall boundary conditions are imposed on the surface of the plate.

First, the distribution of the skin friction coefficient and the turbulence index on the wall surface are shown in Fig. (2) where the transition onset location is at around $x_{\text{cr}} \approx 0.5$ which corresponds to a critical Reynolds number of $\text{Re}_{\text{cr}} \approx 100,000$. Additionally, the contours of amplification factor and intermittency are shown in Fig. (3). As can be seen, the growth of the instabilities lead to the tripping of the boundary layer where the flow becomes turbulent downstream of the transition onset and maintains a turbulent regime for the remainder of the flat plate length.

For the purpose of uncertainty quantification, the friction drag coefficient is used as the quantity of interest. Using the FDOT toolbox[62] for discrete adjoint sensitivity analysis, the flow solver is automatically differentiated such that the sensitivities or gradients of the objective function ($C_{D,f}$) with respect to flow variables as well as the closure coefficients of the AFT transition model can be calculated. The adjoint flow field for the intermittency, i.e., $\overline{\gamma} = \partial C_{D,f}/\partial\gamma$, is shown in Fig. (4). As expected, the sensitivities are largest in the region upstream of the transition onset since tripping of the boundary layer would be the main contributor to the friction drag coefficient. Similarly, the drag coefficient is expected to be almost insensitive to the flow solution downstream of the tripping point. This phenomenon can also be seen in Fig. (5) which shows the distribution of the adjoint solutions along the flat plate wall.

Finally, the normalized adjoints of the closure coefficients of the AFT transition model are presented in Table (2). It is interesting to note that the sensitivities of the friction drag coefficient to these closure coefficients are relatively small. However, it can be noticed that the friction drag coefficient has the highest sensitivity to the c_2 coefficient. As seen before, this closure coefficient directly controls the destruction source term of the intermittency equation (see Eq. [11]). It must be noted that the c_2 closure coefficient also

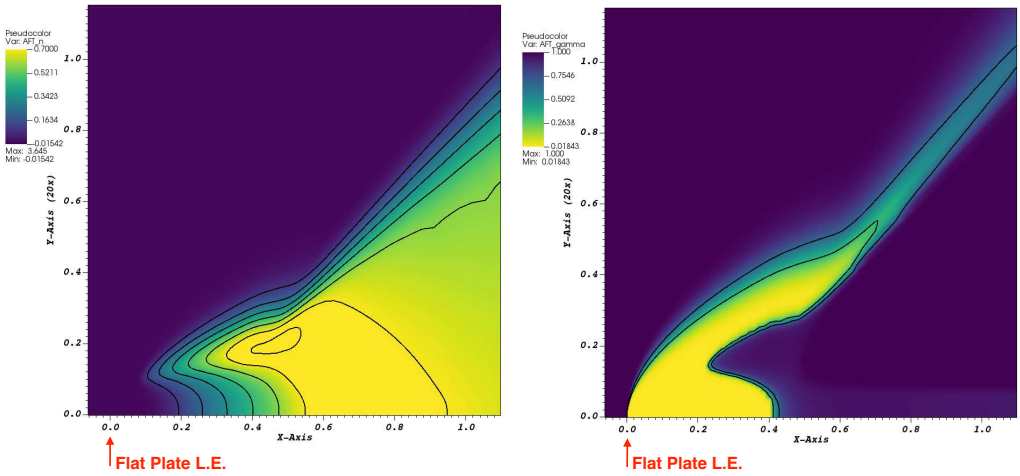

(a) Modified amplification factor, $\tilde{n}$

(b) Original intermittency

Figure 3. Contours of amplification factor and intermittency for the SA-AFT2019 solutions of the modified T3A flat plate case with zero pressure gradient (Tu = 5.855%). Notice the scaling in the normal direction in order to magnify the boundary layer.

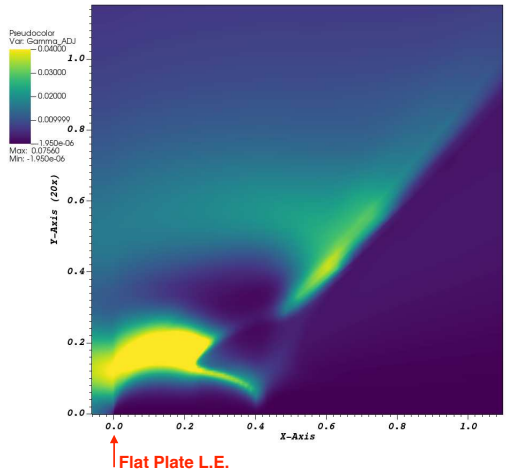

Figure 4. Adjoint field for the intermittency solution, obtained using the "smooth" version of SA-AFT2019 for the modified T3A flat plate case with zero pressure gradient (Tu = 5.855%). Notice the scaling in the normal direction in order to magnify the boundary layer.

happens to have the lowest magnitude compared to the other two closure coefficients (see Table [1]). In fact, the c_2 coefficient is almost four orders of magnitude smaller compared to the c_1 and c_3 coefficients while still leading to the largest sensitivity value for the friction drag coefficient. Therefore, it is safe to assume that calibrating this closure coefficient would have the most significant effects on the transition predictions of the AFT model.

After performing the sensitivity analysis and obtaining discrete adjoint solutions, we can now focus our attention to the actual calibration process for the closure coefficients of the AFT transition model which would be addressed next.

B. Attempt to Calibrate Closure Coefficients of the AFT Transition Model

As was seen in the results of the uncertainty quantification and sensitivity analysis, the transition prediction has the most dependence or sensitivity with respect to the c_2 coefficient that directly controls the destruction

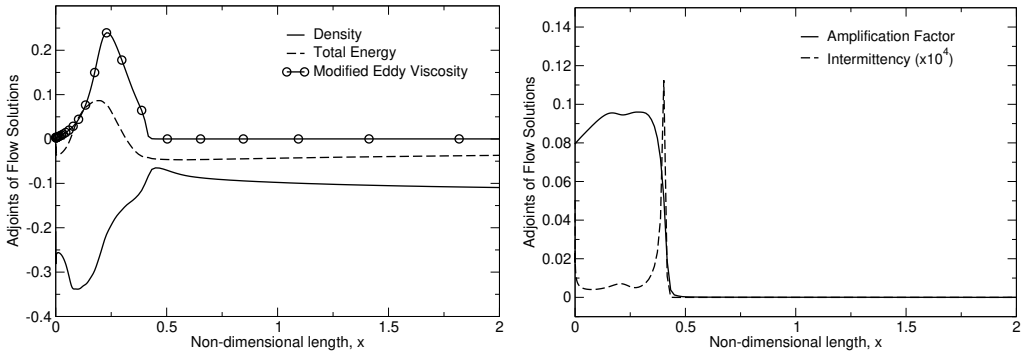

(a) Mean Flow and SA Turbulence Model (b) AFT Transition Model

Figure 5. Adjoints of flow variables along the viscous wall for the modified T3A flat plate case with zero pressure gradient ($\mathbf{Tu} = 5.855\%$) using the smooth version of the SA-AFT2019 model.

Table 2. Adjoints of the closure coefficients for the smooth version of the SA-AFT2019 model for the modified T3A flat plate test case. Here, the friction drag coefficient is used as the quantity of interest for sensitivity analysis.

Adjoint	Value
$\partial C_{D,f}/\partial c_1$	$+7.1180 \times 10^{-6}$
$\partial C_{D,f}/\partial c_2$	-1.3188×10^{-2}
$\partial C_{D,f}/\partial c_3$	-1.7341×10^{-5}

term of the intermittency equation. However, in order to retain the physical behavior of the AFT model in predicting the transition phenomenon, all closure coefficients, including the turbulence Prandtl numbers, i.e., σ_n and σ_γ, will be considered for calibration.

Table 3. Free-stream flow conditions for the standard T3A and T3B zero pressure gradient flat plate test cases.[63]

Case	Re_L	FSTI (Tu%)	Re_c	$x_{\mathrm{cr}}^{\mathrm{target}}/L$
T3A	$360,000$	3.0	$198,000$	0.55
T3B	$630,000$	6.0	$59,850$	0.095

For the purpose of closure coefficient calibration, two standard test cases, known as T3A and T3B, are considered that involve the flow over the flat plate at zero pressure gradient. Both of these cases have a relatively low Reynolds number and a high free-stream turbulence intensity which results in the "bypass" transition through a secondary instability mode. It must be noted that the AFT model, at its core, relies on the linear stability and the e^N models. That makes it well-suited for the "natural" transition phenomenon that is usually associated with much lower values of free-stream turbulence intensity. That being said, in this calibration study, we focus on the two bypass transitional cases in order to examine the effects of closure coefficient calibration on the transition prediction accuracy. For these two cases, the "Extra Fine" mesh from the AIAA TMW's set of recommended grids is utilized that includes 705×384 nodes with 512 grid points along the length of the flat plate. It must be noted that the computational mesh is specifically designed for cases with high free-stream turbulence intensity (FSTI) which makes it suitable for the T3A and T3B cases studied in this work.

Both T3A and T3B cases considered in this section are taken from the ERCOFTAC T3 series[63] with zero pressure gradient. The flow conditions for these two cases are summarized in Table 3. As can be seen, both cases have a low Reynolds number with a relatively high free-stream turbulence intensity which results in a bypass transition of the boundary layer. Additionally, according to the Mack's relation (Eq. [20]), these

FSTI values correspond to relatively low critical amplification factors of $N_{\text{crit}} = 0.86$ and $N_{\text{crit}} = 0.463$ for the T3A and T3B cases, respectively. Additionally, the target transition onset locations for these cases are also provided in Table 3 in terms of the reference length L based on the critical Reynolds number determined from the experimental data. This target location is used in the definition of the objective function (Eq. [25]) which is minimized during the calibration process.

Table 4. Adjoints of the closure coefficients for the standard T3A and T3B flat plate test cases with the objective function defined in terms of the target transition onset location according to Eq. [25].

Adjoint	Value (T3A)	Value (T3B)
$\partial I/\partial c_1$	$+6.865 \times 10^{-6}$	-6.158×10^{-7}
$\partial I/\partial c_2$	-1.200×10^{-2}	$+1.082 \times 10^{-3}$
$\partial I/\partial c_3$	-1.664×10^{-5}	$+1.462 \times 10^{-6}$
$\partial I/\partial \sigma_n$	-9.422×10^{-4}	-2.653×10^{-4}
$\partial I/\partial \sigma_\gamma$	$+3.079 \times 10^{-8}$	-2.196×10^{-9}

The initial sensitivities or gradients of the objective function with respect to the entire set of closure coefficients are presented in Table 4 for the T3A and T3B cases. Once again, it can be noticed that the c_2 coefficient has the largest sensitivity followed by σ_n as the second most sensitive closure coefficient for both cases. However, it is interesting to note that the sign of the gradient for the c_2 coefficient is different for the two bypass transitional cases studied here. The calibration of the closure coefficients is conducted by solving a bound-constrained minimization problem where all design variables are bounded by $\pm 50\%$ of their original value. The convergence of the closure coefficients during the optimization process are shown in Fig. (6) for the T3A and T3B cases.

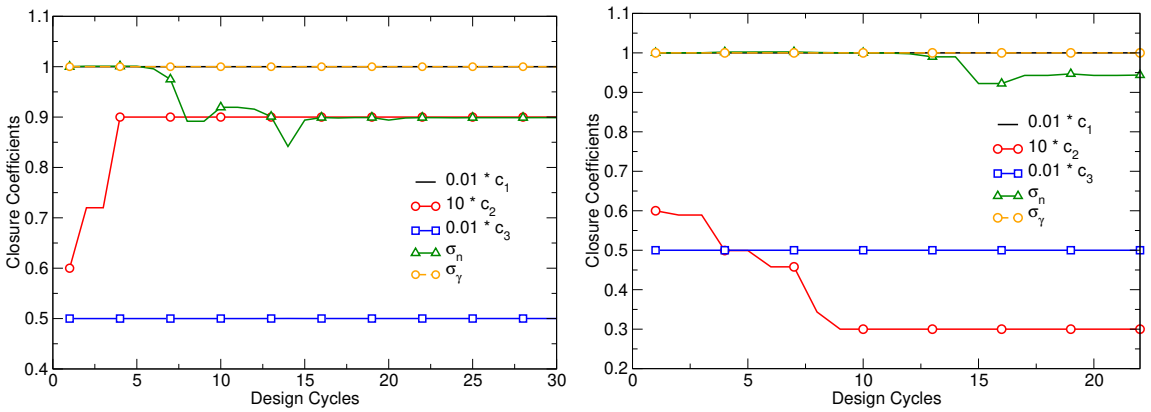

(a) T3A Case (b) T3B Case

Figure 6. Convergence of the closure coefficients during the calibration process via a $\pm 50\%$ bound-constrained minimization problem based on the target onset location.

As expected, the c_2 coefficient, which happens to be the most sensitive of all closure coefficients, experiences the most changes. At the same time, the σ_n coefficient is slightly decreased in both cases. However, as can be seen in Fig. (6), the c_2 coefficient is pushed to its upper bound for the T3A case while it reaches the lower bound for the T3B case which can create an ill-posed design space for the bypass transitional cases studied using the AFT transition model. The final values of the design variables, i.e., the closure coefficients of the AFT model, are presented in Table 5 for the two cases studied in this section. The other three closure coefficients, i.e., c_1, c_3, and σ_γ, barely change during the optimization which can be explained by their small sensitivities (see Table 4).

The direction in which the c_2 coefficient varies inside the design space can be further understood by studying the transition prediction results for the two test cases analyzed in this section. The skin friction

Table 5. Final values of the closure coefficients for the AFT transition model based on the onset location calibration study of the T3A and T3B cases.

Coefficient	Original Value	Optimal Value (T3A)	Optimal Value (T3B)
c_1	100.0	99.9960	100.0005
c_2	0.06	**0.09**	**0.03**
c_3	50.0	50.0088	49.9985
σ_n	1.0	**0.89877**	**0.94384**
σ_γ	1.0	0.99998	1.000001

coefficient profiles for the T3A and T3B cases are shown in Fig. (7). Apparently, for the T3A case, the transition onset location is predicted further upstream of the experimental data while the situation is reversed for the T3B case. Therefore, in the T3A case, the calibration process is seeking to increase the destruction of the intermittency by raising the c_2 coefficient which can ultimately results in delaying the transition phenomenon. On the other hand, for the T3B case, the c_2 coefficient is reduced so that less destruction of the intermittency could potentially result in the boundary layer tripping faster. In the end, due to the conservative bounds that were used for the closure coefficients, the improvements in the transition onset prediction are very insignificant.

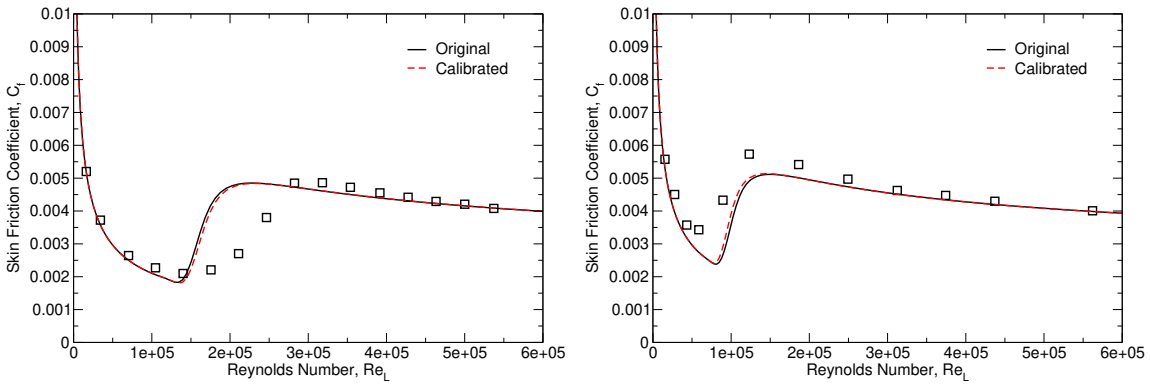

(a) T3A Case

(b) T3B Case

Figure 7. Comparison of the skin friction coefficient profiles obtained using the original and calibrated closure coefficients of the AFT model for the T3A and T3B cases.

Normally, one would seek to identify a universal set of "optimal" closure coefficients that result in improved predictions for a range of benchmark test cases. In the case of the AFT transition model, this can be viewed as an optimal set of closure coefficients for the bypass and/or natural transitional cases. However, for the two bypass transitional cases studied in this section, the main coefficient, i.e., c_2, is pushed in opposite directions which means a "multi-point" optimization of the coefficient would be ill-posed. As a result, it would be improbable if not impossible to obtain an optimal set of coefficients for this class of transition phenomenon. Additionally, it must be once again noted that the AFT model is mainly suited for natural transition cases with low free-stream turbulence intensities. Therefore, the same calibration study can be performed for a set of natural transitional cases to see whether an optimal set of closure coefficients is attainable. This is the subject of an ongoing research and will be addressed in a future study. In the remaining part of this work, however, **we shift our attention to the calibration of the critical amplification factor for the canonical test cases (both bypass and natural transitional) in order to define a newly calibrated relation that could potentially substitute the Mack's relation for the state-of-the-art RANS-based transition prediction studies**.

IV. Calibration of the Critical Amplification Factor

As discussed before, the critical amplification factor, N_{crit}, in the AFT transition model plays a significant role in the prediction of the transition onset. Additionally, this critical factor is directly related to the internal mechanics of the CFD solver.[33] On the other hand, many research studies in the literature that focus on transition prediction using the correlation-based transition models, reportedly modify the free-stream turbulence intensity, which sets the critical amplification factor through Mack's relation, from its experimentally-calculated value in order to reduce the discrepancies between CFD and experimental results.[28,59,60] Therefore, the goal of this study is to use gradient-based optimization to calibrate the critical amplification factor so as to match experimentally reported transition onset location. For this purpose, four canonical test cases are chosen which will be described next. Once the "calibrated" critical amplification factors are determined, those are used to define a new relation similar to Mack's relation.

A. Canonical Flat Plate Test Cases

The four canonical test cases used in this work for the N_{crit} calibration study all involve the zero pressure gradient flat plate flow. The flow conditions as well as the approximate transition onset locations derived from experimental data are reported in Table 6. Note that, two of these cases (T3A and T3B) were used in our attempt to "calibrate" closure coefficients of the AFT model. Additionally, two natural transitional cases are chosen which involve a relatively low free-stream turbulence intensity and a higher Reynolds number. The first natural transitional case is selected from the ERCOFTAC T3 series[63] and is known as the T3A- (also referred to as T3AM). The classical benchmark case of Schubauer-Klebanoff (S&K) is also considered in this work which involves the natural transition of the boundary layer that happens as a result of very low free-stream turbulence intensity.

Table 6. Free-stream flow conditions for the canonical test cases used in the N_{crit} calibration study.

Case	Re_L	FSTI (Tu%)	Re_c	$x_{\text{cr}}^{\text{target}}/L$	Transition Type
T3A	360,000	3.0	198,000	0.55	bypass
T3B	630,000	6.0	63,000	0.10	bypass
T3A-	1,320,000	0.9	1,914,000	1.45	natural
S&K	3,400,000	0.03	3,060,000	0.90	natural

For the calibration of the critical amplification factor, the target transition onset locations described in Table 6 are used in the objective function of Eq. (25). The objective function is minimized using our in-house discrete adjoint-based gradient optimization framework, UNPAC-DOF, that utilizes the smooth version of the SA-AFT2019 model described earlier in this work. The calibration results are shown in Figs. (8) and (9) for the bypass and natural transitional cases in terms of skin friction coefficient profiles. It's seen that the agreements between our predictions and the experimental data are significantly improved with all four cases ultimately calibrating the critical amplification factor to an optimal value that results in the correct prediction of the onset location (according to the experimental data).

Finally, the calibrated values of the critical amplification factor for the four canonical flat plate test cases studied in this section are presented in Table 7. Also presented are the corresponding free-stream turbulence intensities for the calibrated N_{crit} value based on the inverse of the Mack's relation (Eq. [20]). It must be noted that the Mack's relation augmented with the Drela's hyperbolic tangent limiter, is bounded to small but positive values of the critical factor for large turbulence intensities. Therefore, the calibrated N_{crit} value of 0.116 for the T3B case is in fact unattainable with the Mack's relation. However, as was seen in Fig. (8), when the solver is run with the calibrated value of the critical amplification factor, a significant improvement in the prediction of the onset location is achieved.

B. Calibrated Relation for Turbulence Intensity vs. Critical Amplification Factor

With the calibrated values of the critical amplification factor obtained for all four canonical test cases considered in this study, we can now focus on a regression model that can serve as a calibrated relation for determining N_{crit} as a function of the free-stream turbulence intensity that can be used in lieu of Mack's relation. First, the calibrated critical factors for the bypass and natural transitional cases are plotted

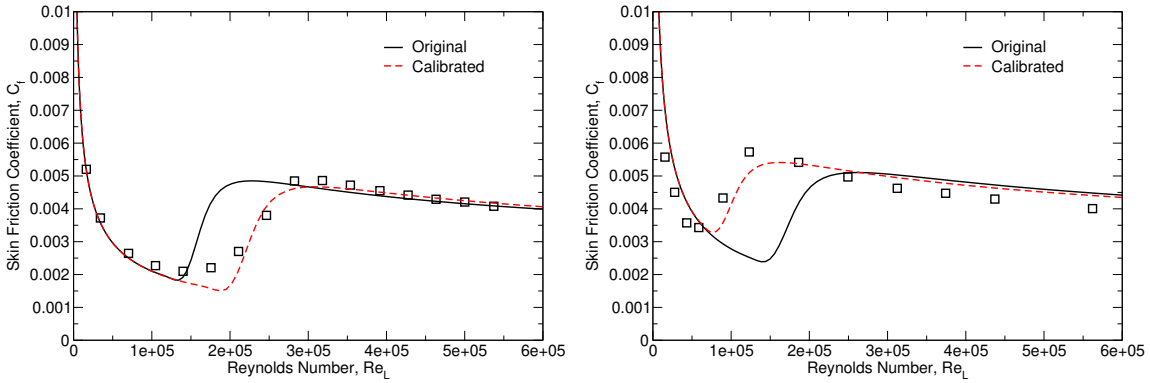

(a) T3A Case

(b) T3B Case

Figure 8. Comparison of the skin friction coefficient profiles obtained using the original and calibrated N_{crit} for the "bypass" transitional cases with experimental data from Ref.[63]

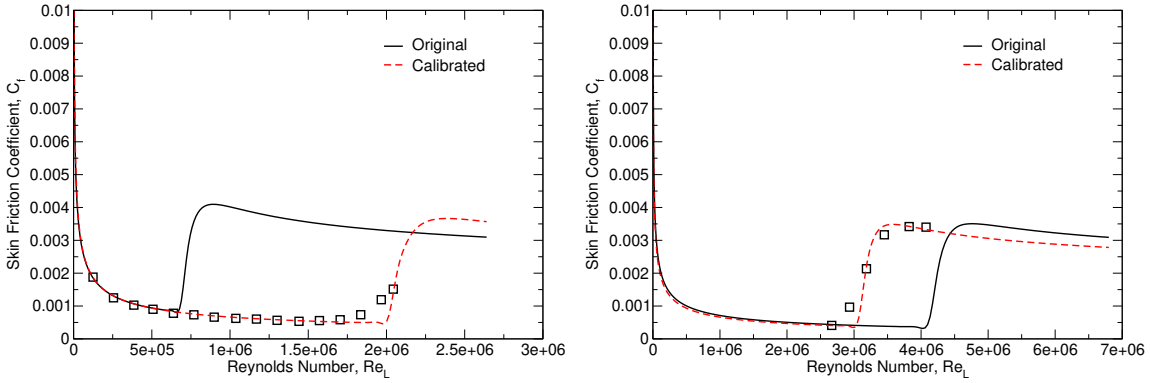

(a) T3A- Case

(b) S&K Case

Figure 9. Comparison of the skin friction coefficient profiles obtained using the original and calibrated N_{crit} for the "natural" transitional cases with experimental data from Refs.[63,64]

Table 7. Original and calibrated critical amplification factors for the canonical flat plate test cases.

Case Name	FSTI (Tu%)	N_{crit} (Mack, Eq. [20])	N_{crit} (Calibrated)	FSTI (Inverse Mack)
T3A	3.0	0.86	1.212	2.268%
T3B	6.0	0.463	0.116	N/A
T3A-	0.9	2.976	5.930	0.253%
S&K	0.03	11.04	7.703	0.1205%

against the Mack's relation and the results are shown in Fig. (10). Also shown are some of the the critical amplification factors that are chosen in the CFD community for improving the transition predictions for these standard test cases. It must be noted that in some of these studies, the authors have simply chosen a different FSTI compared to the reported values from the experimental data. In such cases, the corresponding N_{crit} value obtained from Eq. (20) is shown. Additionally, in studies involving linear stability and e^N models for transition prediction, the actual value of the N_{crit} is shown. It is important to note that our calibrated

critical amplification factors are in line with the typical values used in the CFD community except for the T3A- case where the critical factor is pushed to a significantly higher value. However, to the best of the authors' knowledge, this is the first work reported in the literature that utilizes a gradient-based optimization technique for determining the optimal critical amplification factor in order to calibrate the transition onset location predictions.

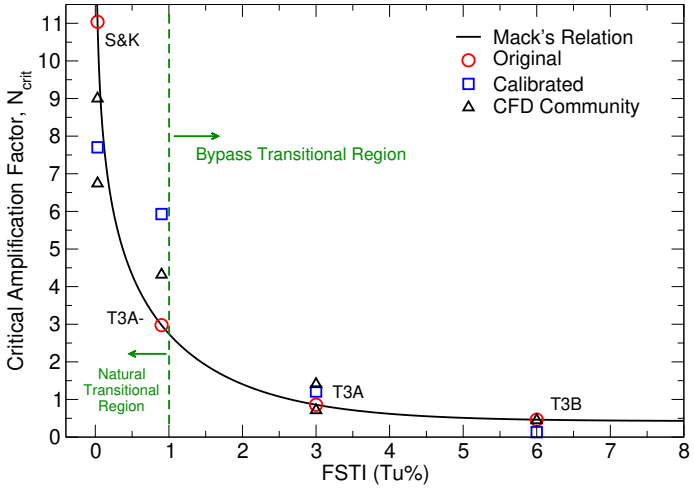

Figure 10. Comparison of the original critical factors, $N_{\mathbf{crit}}$, from the Mack's relation (Eq. [20]) and the calibrated values for the canonical flat plate cases. Also shown are typical $N_{\mathbf{crit}}$ values used in the CFD community.[28, 59, 60]

Prior to fitting a regression model to the calibrated critical factors, it is important to note that our calibrated N_{crit} factors for the natural transitional cases, i.e., S&K and T3A-, show the largest discrepancies with the original values obtained from the Mack's relation. Therefore, a weighted averaging has been utilized to alleviate these discrepancies that could be associated, to some extent, with the challenging nature of these low free-stream turbulence intensity cases. Finally, a fourth-order polynomial regression model is used and the coefficients are obtained using a least-squares optimization method. Additionally, a modification similar to that suggested by Drela[43] is utilized to avoid negative values of the critical amplification factor with a limit of 2.5% as suggested by Coder.[33] The calibrated relation is described as

$$N_{\text{crit}} = a_0 + a_1\tau + a_2\tau^2 + a_3\tau^3 + a_4\tau^4$$
$$\tau = 2.5\tanh\left(\frac{\text{Tu}\%}{2.5}\right) \tag{27}$$

where the coefficients a_0 through a_4 are described in Table 8. It is important to note that the calibrated relation preserves positive values of N_{crit} for a maximum FSTI value of around 10%.

Table 8. Coefficients of the calibrated relation for obtaining the critical amplification factor, $N_{\mathbf{crit}}$, as a function of the free-stream turbulence intensity.

Coefficient	a_0	a_1	a_2	a_3	a_4
Value	9.0064	-4.4958	-1.4208	1.5920	-0.3532

Finally, our newly calibrated regression model is plotted against the Mack's original relation for obtaining the critical amplification factor as a function of the free-stream turbulence intensity and the results are shown in Fig. (11). As can be seen, the calibrated relation agrees well with the critical factor values used by the CFD community although our relation is obtained using a gradient-based calibration process. Additionally, it is important to notice the "exact" fitting of the calibrated factors in the bypass region as opposed to the "approximate" fitting of the calibrated factors in the natural transitional region. In fact, the use of the weighted averaging for the natural transitional region puts our calibrated relation more inline with the critical factors used in other studies reported in the literature.

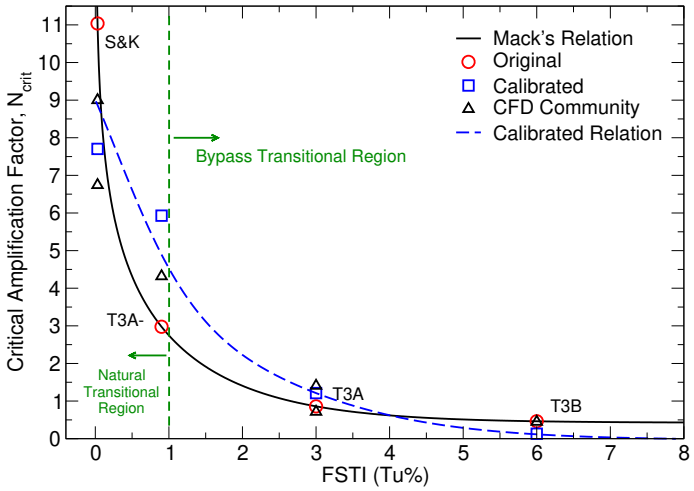

Figure 11. Comparison of our newly calibrated relation for obtaining the critical amplification factor, $N_{\mathbf{crit}}$, as a function of the free-stream turbulence intensity to the original Mack's relation (Eq. [20]).

C. Validation & Verification: NLF(1)-0416 Airfoil

In order to verify the efficacy of the newly calibrated relation for the critical amplification factor, the transitional flow past the NLF(1)-0416 airfoil is considered. The NLF(1)-0416 airfoil was designed with the goal of producing a target maximum lift coefficient that would be roughness-independent while still having a low profile-drag coefficient similar to what is normally achieved with the NACA 6-series airfoils. Additionally, this airfoil is designed to have long runs of laminar flow resulting from favorable pressure gradients along its surface to realize "natural laminar flow".[32] The NLF(1)-0416 test case that will be studied in this work for the purpose of validation and verification (V&V) is subject to a Reynolds number of 4.0 million and a Mach number of 0.1. The free-stream turbulence intensity is set to Tu = 0.045% according to the experimental studies conducted in the NASA Langley Low-Turbulence Pressure Tunnel (LTPT).[8] It must be noted that this free-stream turbulence intensity is also representative of some other low-turbulence wind tunnels such as the Penn State University Low-Speed, Low-Turbulence Wing Tunnel (LSLTT)[65,66] and the Delft University Low-Speed Wind Tunnel (LSWT)[67] that are all designed for very high critical amplification factors.[32]

1. Grid Convergence Study

In order to make sure that the numerical results are grid converged, four different grid resolutions are considered and the grid convergence studies are conducted. These C-typed structured computational grids are provided by the AIAA TMW (Case 2) and are extended to 1000-chord units away from the airfoil. The four grid resolutions (levels L0 through L3) are shown in Fig. (12) where the number of grids nodes around the circumference of the airfoil varies from 512 for the "Medium" (L3) grid to 1536 for the "Ultra Fine" (L0) grid.

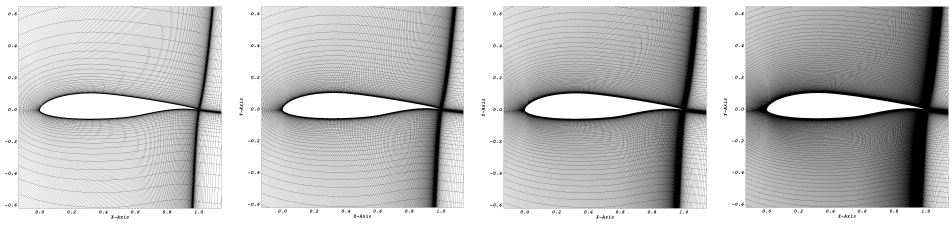

(a) L3 Grid (b) L2 Grid (c) L1 Grid (d) L0 Grid

Figure 12. Computational grids for the transitional flow past the NLF(1)-0416 airfoil.

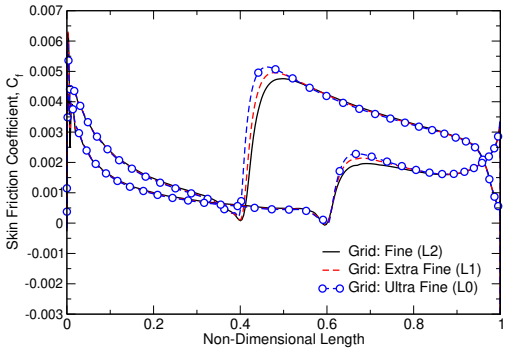

Figure 13. Grid convergence study in terms of skin friction coefficient for the transitional flow past the NLF(1)-0416 airfoil at 0-deg angle of attack.

For the purpose of grid convergence study, the free-stream flow at a zero degree angle of attack with a free-stream turbulence intensity of 0.045% is considered and the results in terms of the skin friction profile are shown in Fig. (13) for the finest grid levels, i.e., L0 through L2. As can be seen, all skin friction profiles are very similar with distinct differences in the vicinity of the transition onset location. On the other hand, the convergence of the lift and drag coefficients with respect to the grid resolution is studied and the results are shown in Fig. (14). It is important to note that both the lift coefficient as well as the drag count converge as the grid resolution is increased. Additionally, the results of the grid convergence study are presented in Table (9) which also include the differences (in percent) compared to the results obtained on the finest grid, i.e., the "Ultra Fine" (L0). It can be clearly seen that the differences between the L1 and L0 grids in terms of lift and drag coefficients are small. Therefore, the L1 grid is ultimately chosen for the rest of the results presented in this section.

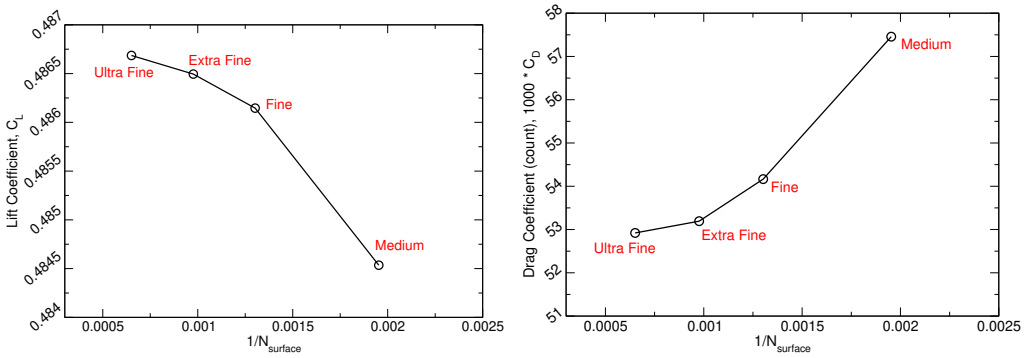

(a) Lift Coefficient

(b) Drag Coefficient (count)

Figure 14. Grid convergence study in terms of lift coefficient and drag count for the transitional flow past the NLF(1)-0416 airfoil at 0-deg angle of attack.

Table 9. Results of the grid convergence study in terms of lift coefficient and drag count for the transitional flow past the NLF(1)-0416 airfoil at 0-deg angle of attack.

Grid	N_{surf}	$1/N_{\text{surf}}$	C_L	Diff. (%)	C_D (count)	Diff. (%)
Medium (L3)	512	0.00195	0.484535	0.44	57.457	8.57
Fine (L2)	768	0.00130	0.486146	0.11	54.165	2.35
Extra Fine (L1)	1024	0.00097	0.486495	0.04	53.193	0.51
Ultra Fine (L0)	1536	0.00065	0.486686	-	52.921	-

2. *Lift, Drag, and Transition Predictions*

As discussed earlier, the value of the free-stream turbulence intensity for this case is Tu = 0.045% according to the experimental data. However, in many research studies available in the literature, the value of the FSTI is increased to 0.15% since the transition onset locations are consistently predicted further downstream of those reported by the experiment.[50,58] This was first reported by Coder[32] and resulted in a significant improvement of the transition predictions compared to the experimental data for the NLF(1)-0416 airfoil in a wide range of angles of attack. It must be noted that the FSTI of 0.045% corresponds to a critical amplification factor of $N_{\text{crit}} = 10.07$ according to the Mack's relation (Eq. [20]). Therefore, by increasing the value of FSTI, the critical amplification factor is in fact reduced to $N_{\text{crit}} = 7.18$ (equivalent to Tu = 0.15% according to Eq. [20]).[32]

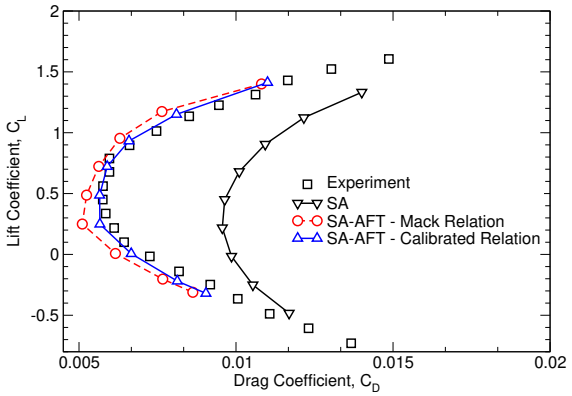

Figure 15. Drag polar for angles of attack from -8 to 8 degrees for the turbulent (SA) and transitional (SA-AFT) cases using the original Mack's and the newly calibrated relations: NLF(1)-0416 airfoil at Re $= 4.0 \times 10^6$**,** $M_\infty = 0.1$**, and Tu** $= 0.045\%$**. Experimental data is obtained from Ref.[8]**

In this work, however, the goal is to use the newly calibrated relation instead of the Mack's relation while still using the experimental value of the free-stream turbulence intensity, i.e., Tu = 0.045%. This value of FSTI is equivalent to a critical amplification factor of $N_{\text{crit}} = 8.8$ according to our new relation (Eq. [27]). The drag polar for the NLF(1)-0416 airfoil at $\text{Re} = 4 \times 10^6$ and $M = 0.1$ for an AoA sweep between $[-8, 8]$ deg is shown in Fig. (15). While in general, the SA-AFT transitional results have consistently increased the accuracy of the lift and drag predictions compared to the fully-turbulent solutions (obtained via SA-neg model), the agreements with the experimental data are significantly improved with the newly calibrated relation. This was expected since the value of the critical amplification factor is reduced from that obtained using the Mack's relation which results in the expedition of the transition onset and thus, the slight increase in the friction drag coefficients.

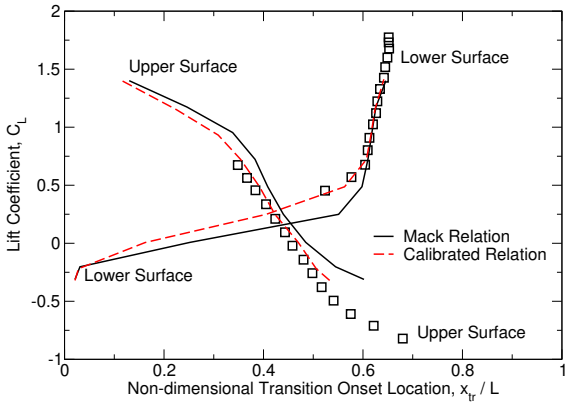

Figure 16. Transition onset predictions on the top and bottom surfaces of the NLF(1)-0416 airfoil for the transitional (SA-AFT) simulations using the original Mack's and the newly calibrated relations: at Re $= 4.0 \times 10^6$**,** $M_\infty = 0.1$**, and Tu** $= 0.045\%$**. Experimental data (represented with square symbols) is obtained from Ref.[32]**

Additionally, the transition onset locations on the top and bottom surfaces of the NLF airfoil are predicted according to the turbulence index profile and the results are shown in Fig. (16). As can be seen, the transition predictions using the newly calibrated value of the critical amplification factor agree much more closely with experiment compared to those obtained from the Mack's relation for all lift coefficients. Once again, this result was expected since the reduction of the critical amplification factor according to the newly calibrated relation would lead to the transition onset points consistently shifting toward the leading edge of the airfoil.

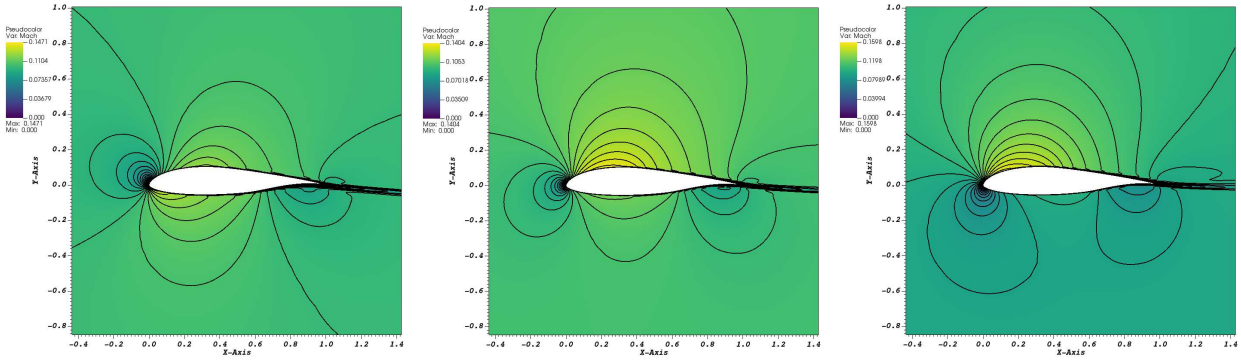

(a) AoA = -4 deg (b) AoA = 0 deg (c) AoA = +4 deg

Figure 17. Contours of Mach number for transitional flow around NLF(1)-0416 airfoil at various angles of attack, Re $= 4.0 \times 10^6$, $M_\infty = 0.1$, and Tu $= 0.045\%$, using the newly calibrated relation.

Finally, the flow solutions for various angles of attack in terms of Mach number and intermittency are shown in Figs. (17) and (18), respectively. Additionally, the eddy viscosity ratio, μ_t/μ, solutions are presented for the zero angle of attack (AoA) case with fully-turbulent (SA) and transitional (SA-AFT2019) assumptions based on the newly calibrated value of the $N_{\text{crit}} = 8.8$ and the results are shown in Fig. (19). As can be seen, turbulence in the boundary layer of the NLF(1)-0416 is remarkably over-predicted with the fully-turbulent assumption while the maximum eddy viscosity ratio is almost halved in the transitional flow obtained using the SA-AFT2019 model.

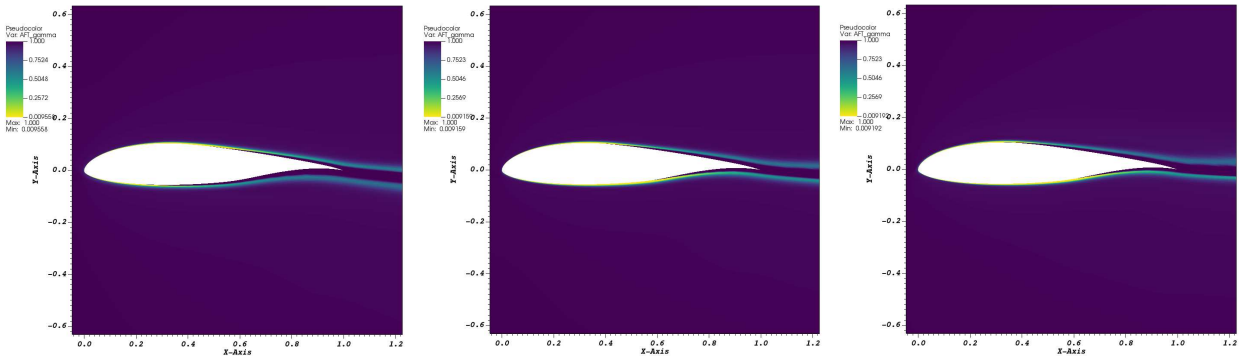

(a) AoA = -4 deg (b) AoA = 0 deg (c) AoA = +4 deg

Figure 18. Contours of intermittency (γ) for transitional flow around NLF(1)-0416 airfoil at various angles of attack, Re $= 4.0 \times 10^6$, $M = 0.1$, and Tu $= 0.045\%$, using the newly calibrated relation.

V. Conclusions

A gradient-based optimization framework was used for uncertainty quantification and sensitivity analysis of the two-equation Amplification Factor Transport (AFT) transition model. The goal of the sensitivity

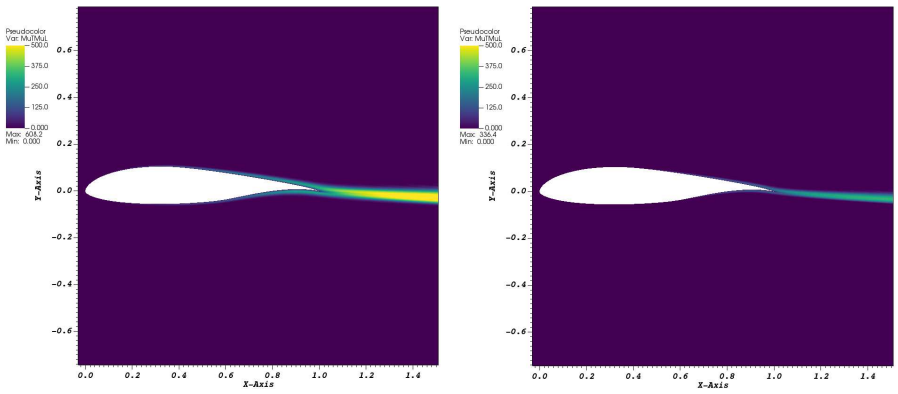

(a) Turbulent Flow (b) Transitional Flow

Figure 19. Contours of eddy viscosity ratio, μ_t/μ_l, for turbulent and transitional flows around NLF(1)-0416 airfoil at zero degree angle of attack, Re $= 4.0 \times 10^6$, $M_\infty = 0.1$, and Tu $= 0.045\%$, using the newly calibrated relation.

analysis was to identify the most sensitive closure coefficients of the model that can directly affect the transition prediction capabilities for various transitional test cases. Additionally, the critical amplification factor in the source term of the intermittency equation was calibrated via an adjoint-based optimization of the transition onset location based on the experimental data. To the best of the authors' knowledge, this was the first work that addressed the calibration of the critical amplification factor using a gradient-based approach that could efficiently identify the N_{crit} values for various bypass and natural transitional test cases. For this purpose, four canonical flat plate test cases were considered. These were based on the experimental studies of the ERCOFTAC T3 series[63] as well as the Schubauer-Klebanoff (S&K).[64] Moreover, the transition onset location was represented by a sigmoid function of the turbulence index profile which resulted in a smooth and differentiable design space that is essential to the discrete adjoint approach. Ultimately, a regression model approach was used to determine a new relation for determining the critical amplification factor as a function of the free-stream turbulence intensity for a wide range of FSTI values. Finally, the efficacy of the newly calibrated relation was verified by modeling the transitional boundary layer of the natural laminar flow NLF(1)-0416 airfoil in a wide range of angles of attack. The results showed significant improvements in predicting the transition onset location as well as lift and drag coefficients compared to those obtained from the original Mack's relation.[42,43]

VI. Acknowledgments

This material is based upon work supported by the National Science Foundation under grant No: CBET-1803760. The authors greatly appreciate the support provided.

References

[1]Slotnick, J., Khodadoust, A., Alonso, J., Darmofal, D., Gropp, W., Lurie, E., and Mavriplis, D., "CFD vision 2030 study: a path to revolutionary computational aerosciences," 2014.

[2]Xiao, H. and Cinnella, P., "Quantification of model uncertainty in RANS simulations: A review," *Progress in Aerospace Sciences*, Vol. 108, 2019, pp. 1–31.

[3]Duraisamy, K., Iaccarino, G., and Xiao, H., "Turbulence modeling in the age of data," *Annual Review of Fluid Mechanics*, Vol. 51, 2019, pp. 357–377.

[4]Duraisamy, K., "Machine Learning-augmented Reynolds-averaged and Large Eddy Simulation Models of Turbulence," *arXiv preprint arXiv:2009.10675*, 2020.

[5]Spalart, P. and Allmaras, S., "A one-equation turbulence model for aerodynamic flows," AIAA Paper 1992-439, 1992.

[6]Allmaras, S. R. and Johnson, F. T., "Modifications and clarifications for the implementation of the Spalart-Allmaras turbulence model," *Seventh international conference on computational fluid dynamics (ICCFD7)*, 2012, pp. 1–11.

[7]Medida, S., *Correlation-based transition modeling for external aerodynamic flows*, Ph.D. thesis, 2014.

[8]Somers, D. M., "Design and experimental results for a natural-laminar-flow airfoil for general aviation applications," *NASA Technical Paper (1861)*, 1981.

[9]Langtry, R. and Menter, F., "Transition modeling for general CFD applications in aeronautics," *AIAA paper*, Vol. 522, No. 2005, 2005, pp. 14.

[10]Langtry, R. B. and Menter, F. R., "Correlation-based transition modeling for unstructured parallelized computational fluid dynamics codes," *AIAA Journal*, Vol. 47, No. 12, 2009, pp. 2894–2906.

[11]Lee, J.-D. and Jameson, A., "Natural-laminar-flow airfoil and wing design by adjoint method and automatic transition prediction," AIAA Paper 2009-0897, 2009.

[12]Hanifi, A., Amoignon, O., Pralits, J. O., and Chevalier, M., "A gradient-based optimization method for natural laminar flow design," *Seventh IUTAM Symposium on Laminar-Turbulent Transition*, Springer, 2010, pp. 3–10.

[13]Campbell, R. L., Campbell, M. L., and Streit, T., "Progress toward efficient laminar flow analysis and design," AIAA Paper 2011-3527, 2011.

[14]Cameron, L., Early, J., and McRoberts, R., "Metamodel Assisted Multi-Objective Global Optimisation of Natural Laminar Flow Aerofoils," AIAA Paper 2011-3001, 2011.

[15]Khayatzadeh, P. and Nadarajah, S. K., "Aerodynamic Shape Optimization via Discrete Viscous Adjoint Equations for the k- ω SST Turbulence and γ-Re$_{\theta t}$ Transition Models," AIAA Paper 2011-1247, 2011.

[16]Khayatzadeh, P. and Nadarajah, S. K., "Aerodynamic shape optimization of natural laminar flow (NLF) airfoils," AIAA Paper 2012-0061, 2012.

[17]Coder, J. G. and Maughmer, M. D., "A CFD-compatible transition model using an amplification factor transport equation," AIAA Paper 2013-0253, 2013.

[18]Howison, J. and Ekici, K., "Dynamic stall analysis using harmonic balance and correlation-based γ-Re$_{\theta t}$ transition models for wind turbine applications," *Wind Energy*, Vol. 18, No. 12, 2015, pp. 2047–2063.

[19]Arnal, D., Casalis, G., and Houdeville, R., "Practical transition prediction methods: subsonic and transonic flows," *VKI Lectures Series Advances in Laminar-Turbulent Transition Modelling*, 2008.

[20]Medida, S., *Correlation-based Transition Modeling for External Aerodynamic Flows*, Ph.D. thesis, University of Maryland College Park, 2014.

[21]Smith, A. M. O., "Transition, pressure gradient and stability theory," *Douglas Aircraft Co., Report ES 26388*, 1956.

[22]Van Ingen, J., "A suggested semi-empirical method for the calculation of the boundary layer transition region," *Technische Hogeschool Delft, Vliegtuigbouwkunde, Rapport VTH-74*, 1956.

[23]Rashad, R. and Zingg, D. W., "Aerodynamic Shape Optimization for Natural Laminar Flow Using a Discrete-Adjoint Approach," *AIAA Journal*, 2016.

[24]Mayle, R., "The role of laminar-turbulent transition in gas turbine engines," *Journal of Turbomachinery*, Vol. 113, 1991, pp. 509–537.

[25]Abu-Ghannam, B. and Shaw, R., "Natural transition of boundary layers—the effects of turbulence, pressure gradient, and flow history," *Journal of Mechanical Engineering Science*, Vol. 22, No. 5, 1980, pp. 213–228.

[26]Menter, F. R., "Two-equation eddy-viscosity turbulence models for engineering applications," *AIAA Journal*, Vol. 32, No. 8, 1994, pp. 1598–1605.

[27]Medida, S. and Baeder, J. D., "Application of the correlation-based γ-Re$_{\theta t}$ transition model to the Spalart-Allmaras turbulence model," AIAA Paper 2011-3979, 2011.

[28]Bas, O., Cakmakcioglu, S. C., and Kaynak, U., "A novel intermittency distribution based transition model for low-Re number airfoils," AIAA Paper 2013-2531, 2013.

[29]Di Pasquale, D., Rona, A., and Garrett, S., "A selective review of CFD transition modelling," *39th AIAA fluid dynamics conference*, 2009, p. 3812.

[30]Smith, A. and Gamberoni, N., "Transition, pressure gradient and stability theory," *Douglas Aircraft Rept. ES-26388*, 1956.

[31]Van Ingen, J., "A suggested semi-empirical method for the calculation of the boundary layer transition region," *Technische Hogeschool Delft, Vliegtuigbouwkunde, Rapport VTH-74*, 1956.

[32]Coder, J. G., *Development of a CFD-compatible transition model based on linear stability theory*, Ph.D. thesis, The Pennsylvania State University, 2014.

[33]Coder, J. G., "Further development of the amplification factor transport transition model for aerodynamic flows," AIAA Paper 2019-0039, 2019.

[34]Langtry, R. B. and Menter, F. R., "Correlation-based transition modeling for unstructured parallelized computational fluid dynamics codes," *AIAA journal*, Vol. 47, No. 12, 2009, pp. 2894–2906.

[35]Thévenin, D. and Janiga, G., *Optimization and computational fluid dynamics*, Springer Science & Business Media, Berlin, Heidelberg, 2008.

[36]Edeling, W. N., Schmelzer, M., Dwight, R. P., and Cinnella, P., "Bayesian predictions of Reynolds-averaged Navier–Stokes uncertainties using maximum a posteriori estimates," *AIAA Journal*, Vol. 56, No. 5, 2018, pp. 2018–2029.

[37]Oliver, T. A. and Moser, R. D., "Bayesian uncertainty quantification applied to RANS turbulence models," *Journal of Physics: Conference Series*, Vol. 318, IOP Publishing, 2011, p. 042032.

[38]Zhao, Y., Yan, C., Wang, X., Liu, H., and Zhang, W., "Uncertainty and sensitivity analysis of SST turbulence model on hypersonic flow heat transfer," *International Journal of Heat and Mass Transfer*, Vol. 136, 2019, pp. 808–820.

[39]Schaefer, J., Hosder, S., West, T., Rumsey, C., Carlson, J.-R., and Kleb, W., "Uncertainty quantification of turbulence model closure coefficients for transonic wall-bounded flows," *AIAA Journal*, Vol. 55, No. 1, 2017, pp. 195–213.

[40]Di Stefano, M. A., Hosder, S., and Baurle, R. A., "Effect of Turbulence Model Uncertainty on Scramjet Isolator Flowfield Analysis," *Journal of Propulsion and Power*, Vol. 36, No. 1, 2020, pp. 109–122.

[41]Erb, A. and Hosder, S., "Analysis of Turbulence Model Uncertainty for Shock-Wave/Boundary-Layer Interaction Simulations," *Journal of Spacecraft and Rockets*, 2020, pp. 1–20.

[42]Mack, L., "Transition and laminar instability. JPL Publication 77-15," *Jet Propulsion Laboratory, California Institute of Technology, Pasadena, California, USA*, 1977.

[43]Drela, M., "MISES implementation of modified Abu-Ghannam/Shaw transition criterion (second revision)," *Massachusetts Institute of Technology Dept. of Aeronautics and Astronautics*, 1998.

[44]Coder, J. G. and Maughmer, M. D., "Computational fluid dynamics compatible transition modeling using an amplification factor transport equation," *AIAA journal*, Vol. 52, No. 11, 2014, pp. 2506–2512.

[45]Coder, J. G., "Enhancement of the Amplification Factor Transport Transition Modeling Framework," AIAA Paper 2017-1709, 2017.

[46]Drela, M. and Giles, M. B., "Viscous-inviscid analysis of transonic and low Reynolds number airfoils," *AIAA journal*, Vol. 25, No. 10, 1987, pp. 1347–1355.

[47]Denison, M. and Pulliam, T. H., "Implementation and Assessment of the Amplification Factor Transport Laminar-Turbulent Transition Model," AIAA Paper 2018-3382, 2018.

[48]Coder, J. G., Pulliam, T. H., and Jensen, J. C., "Contributions to HiLiftPW-3 using structured, overset grid methods," AIAA Paper 2018-1039, 2018.

[49]Menter, F. R., Smirnov, P. E., Liu, T., and Avancha, R., "A one-equation local correlation-based transition model," *Flow, Turbulence and Combustion*, Vol. 95, No. 4, 2015, pp. 583–619.

[50]Halila, G. L., Martins, J. R., and Fidkowski, K. J., "Adjoint-based aerodynamic shape optimization including transition to turbulence effects," *Aerospace Science and Technology*, Vol. 107, 2020, pp. 106243.

[51]Shimoda, M., Azegami, H., and Sakurai, T., "Numerical Solution for Min-Max Shape Optimization Problems: Minimum Design of Maximum Stress and Displacement," *JSME International Journal Series A Solid Mechanics and Material Engineering*, Vol. 41, No. 1, 1998, pp. 1–9.

[52]Poon, N. M. and Martins, J. R., "An adaptive approach to constraint aggregation using adjoint sensitivity analysis," *Structural and Multidisciplinary Optimization*, Vol. 34, No. 1, 2007, pp. 61–73.

[53]Wang, Y., Zhang, Y., Li, S., and Meng, D., "Calibration of a γ-Re_θ transition model and its validation in low-speed flows with high-order numerical method," *Chinese Journal of Aeronautics*, Vol. 28, No. 3, 2015, pp. 704–711.

[54]Colonia, S., Leble, V., Steijl, R., and Barakos, G., "Assessment and Calibration of the γ-Equation Transition Model at Low Mach," *AIAA Journal*, Vol. 55, No. 4, 2017, pp. 1126–1139.

[55]Abd Bari, M. A., Da Ronch, A., Panzeri, M., and Drofelnik, J., "On the calibration of the intermittency transition turbulence model for wind turbine airfoil by machine learning algorithm," *31st Congress of the International Council of the Aeronautical Sciences, Belo Horizonte, Brazil*, 2019.

[56]Nader, G., dos Santos, C., Jabardo, P. J., Cardoso, M., Taira, N. M., and Pereira, M. T., "Characterization of low turbulence wind tunnel," *XVIII IMEKO World Congress, Rio de Janeiro, Brazil, September*, 2006.

[57]Scheiman, J. and Kubendran, L., "Laser velocimeter measurements in a wing-fuselage type juncture," *NASA Technical Paper (100588)*, 1988.

[58]Shi, Y., Mader, C. A., He, S., Halila, G. L., and Martins, J. R., "Natural Laminar-Flow Airfoil Optimization Design Using a Discrete Adjoint Approach," *AIAA Journal*, Vol. 58, No. 11, 2020, pp. 4702–4722.

[59]Barrouillet, B., Laurendeau, E., and Yang, H., "On the calibration of the transitional k-ω-γ-$\mathrm{Re}_{\theta t}$ turbulence model," AIAA Paper 2021-0629, 2021.

[60]Lee, B. and Baeder, J. D., "Prediction and validation of laminar-turbulent transition using SA-γ transition model," AIAA Paper 2021-1532, 2021.

[61]Djeddi, S., *Towards Adaptive and Grid-Transparent Adjoint-Based Design Optimization Frameworks*, Ph.D. thesis, University of Tennessee, 2018.

[62]Djeddi, R. and Ekici, K., "FDOT: A Fast, Memory-Efficient and Automated Approach for Discrete Adjoint Sensitivity Analysis using the Operator Overloading Technique," *Aerospace Science and Technology*, Vol. 91, 2019, pp. 159–174.

[63]Coupland, J., "ERCOFTAC special interest group on laminar to turbulent transition and retransition: T3A and T3B test cases," Tech. Rep. A309514, 1990.

[64]Schubauer, G. B. and Klebanoff, P. S., "Contributions on the mechanics of boundary-layer transition," 1956.

[65]Brophy, C. M., *Turbulence management and flow qualification of the Pennsylvania State University Low-Turbulence, Low-Speed, closed-circuit wind tunnel*, Ph.D. thesis, Pennsylvania State University, 1994.

[66]Premi, A., Maughmer, M., and Brophy, C., "Flow-quality measurements and qualification of the Pennsylvania State University Low-Speed, Low-Turbulence wind tunnel," AIAA Paper 2012-1214, 2012.

[67]Van Ingen, J., Boermans, L., and Blom, J., "Low-speed airfoil section research at Delft University of Technology," *12th Congress of the International Council of the Aeronautical Sciences*, 1980.